A computational perspective on autism

Ari Rosenberg[1], Jaclyn Sky Patterson, and Dora E. Angelaki[1]

Department of Neuroscience, Baylor College of Medicine, Houston, TX 77030

This contribution is part of the special series of Inaugural Articles by members of the National Academy of Sciences elected in 2014.

Contributed by Dora E. Angelaki, May 29, 2015 (sent for review February 25, 2015; reviewed by Odelia Schwartz and Reza Shadmehr)

Autism is a neurodevelopmental disorder that manifests as a heterogeneous set of social, cognitive, motor, and perceptual symptoms. This system-wide pervasiveness suggests that, rather than narrowly impacting individual systems such as affection or vision, autism may broadly alter neural computation. Here, we propose that alterations in nonlinear, canonical computations occurring throughout the brain may underlie the behavioral characteristics of autism. One such computation, called divisive normalization, balances a neuron's net excitation with inhibition reflecting the overall activity of the neuronal population. Through neural network simulations, we investigate how alterations in divisive normalization may give rise to autism symptomatology. Our findings show that a reduction in the amount of inhibition that occurs through divisive normalization can account for perceptual consequences of autism, consistent with the hypothesis of an increased ratio of neural excitation to inhibition (E/I) in the disorder. These results thus establish a bridge between an E/I imbalance and behavioral data on autism that is currently absent. Interestingly, our findings implicate the context-dependent, neuronal milieu as a key factor in autism symptomatology, with autism reflecting a less "social" neuronal population. Through a broader discussion of perceptual data, we further examine how altered divisive normalization may contribute to a wide array of the disorder's behavioral consequences. These analyses show how a computational framework can provide insights into the neural basis of autism and facilitate the generation of falsifiable hypotheses. A computational perspective on autism may help resolve debates within the field and aid in identifying physiological pathways to target in the treatment of the disorder.

autism | neural computation | divisive normalization | E/I imbalance | Bayesian inference

Autism is a neurodevelopmental disorder that is dramatically increasing in prevalence (Fig. 1). Recent data place the number of children being diagnosed with autism in the United States at 1 in 68, more than doubling in the last decade (1–4). The disorder is highly pervasive, affecting individuals at cognitive, motor, and perceptual levels. It is furthermore a "spectrum disorder," with symptoms that manifest in varying degrees across individuals. This heterogeneity presents significant challenges to establishing a comprehensive characterization of the disorder.

Research investigating the genetic and molecular basis of autism implicates over 100 genes (5), many of which are involved in synaptic development and function (6–8). As such, one prominent hypothesis is that autism arises from a neurophysiological excitation-to-inhibition (E/I) imbalance (9, 10). However, the connection between an E/I imbalance and the behavioral characteristics of the disorder remains unclear. Considering the pervasive nature of autism, and the covariance of loosely related symptoms (11–14), one possibility is that an E/I imbalance widely affects neural computation, in turn giving rise to the broad behavioral symptoms recognized as autism.

Here, we propose that autism symptomatology arises from alterations in nonlinear, canonical computations occurring throughout the brain; in particular, divisive normalization, a computation that divides the activity of individual neurons by the combined activity of the neuronal population in which they are embedded. Divisive normalization inherently reflects the E/I balance, and is implicated in a wide range of processes ranging from sensory encoding to decision making (15–17). Using neural network simulations, we show that a reduction in the amount of inhibition that occurs through divisive normalization can account for perceptual consequences reported in the disorder, providing a bridge between an E/I imbalance and the behavioral characteristics of autism. The simulations further establish a link between divisive normalization and high-level theories about how autism may alter the influence of past experience on the interpretation of current sensory information (18–20). A key result of the simulations is the implication of the neuronal milieu (the contextual environment of neuronal population activity in which neurons are embedded) in autism. Specifically, autism-like symptomatology arises in the model when the influence of the population on the activity of individual neurons is reduced, in essence making the neurons less "social." A broader discussion of behavioral data further suggests that alterations in divisive normalization may contribute to the phenotypic diversity of autism.

Evidence for an E/I Imbalance in Autism

In this section, we briefly discuss evidence linking autism to a neurophysiological E/I imbalance. Excitatory (e.g., glutamatergic) and inhibitory (e.g., GABAergic) neurons together establish an E/I balance that is essential for normal brain development and function (21). This E/I balance plays an important role in determining the timing of critical periods in neurodevelopment. For example, GABA-mediated inhibition is important for determining the critical period in primary visual cortex (22), and experience-dependent plasticity is altered in mice lacking GAD, an enzyme involved in converting glutamate to GABA (23).

Significance

Autism is a pervasive disorder that broadly impacts perceptual, cognitive, social, and motor functioning. Across individuals, the disorder manifests with a large degree of phenotypic diversity. Here, we propose that autism symptomatology reflects alterations in neural computation. Using neural network simulations, we show that a reduction in the amount of inhibition occurring through a computation called divisive normalization can account for perceptual consequences reported in autism, as well as proposed changes in the extent to which past experience influences the interpretation of current sensory information in individuals with the disorder. A computational perspective can help bridge our understandings of the genetic/molecular basis of autism and its behavioral characteristics, providing insights into the disorder and possible courses of treatment.

Author contributions: A.R. and D.E.A. designed research; A.R. and J.S.P. performed research; A.R. and J.S.P. analyzed data; and A.R., J.S.P., and D.E.A. wrote the paper.

Reviewers: O.S., University of Miami; and R.S., Johns Hopkins University.

The authors declare no conflict of interest.

[1]To whom correspondence may be addressed. Email: ari.rosenberg@wisc.edu or angelaki@bcm.edu.

This article contains supporting information online at www.pnas.org/lookup/suppl/doi:10.1073/pnas.1510583112/-/DCSupplemental.

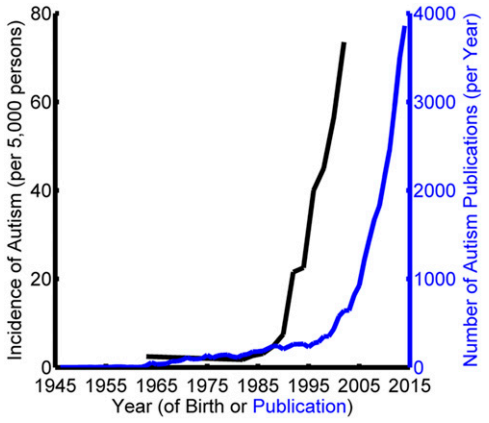


Fig. 1. Increasing prevalence of autism and research on the disorder. The incidence of autism (black curve) is compiled from studies by Wing and Gould (1), Newschaffer et al. (2), and the Centers for Disease Control and Prevention (3, 4). Paralleling this rapid rise in prevalence is increased research on the disorder. The number of publications in which "autism" appears in any PubMed field (blue curve) is shown for every year from 1946 to 2014.

Such findings suggest that an E/I imbalance can alter neurodevelopment, but is this related to autism?

One hypothesis proposes that autism symptomatology arises from an increased E/I ratio (9, 10), which may explain the frequent comorbidity of the disorder and seizures (24). An E/I imbalance in autism may originate in several ways including increased glutamate activity (25), decreased GABA release (7, 8), or decreased numbers of GABA receptors (26). Consistent with the possibility of an E/I imbalance in autism, many of the susceptibility genes may be related to the E/I balance. A few examples include single-nucleotide polymorphisms at chromosome 6q21, which encodes a glutamate receptor (27), the gene for the β3 $GABA_A$ receptor subunit (28), and MeCP2, which is critical for GABAergic function (7).

An increased E/I ratio is also supported by biochemical analyses. For example, decreased GABA receptor protein subunits are reported in autism (29, 30). Histological analysis further shows decreased mRNA levels of the enzyme GAD in autism (31, 32), and mice lacking GAD have decreased GABA levels (23). In a mouse model of autism with increased translation of neuroligins, both an increased E/I ratio and autistic-like behaviors are observed (33). In the next section, we describe divisive normalization, a canonical neural computation that is inherently related to the balance of excitation and inhibition. We then use divisive normalization to establish a computational bridge between an increased E/I ratio and autism symptomatology.

Connecting the E/I Balance to Neural Computation

We refer to stereotyped functions occurring throughout the brain as "canonical computations." One such computation is divisive normalization, which divides the net excitatory drive to a neuron by a measure of the population activity (15). The effect of divisive normalization on a single neuron's response is described by the following equation:

$$R = \frac{D}{\nu + c \cdot S}. \qquad [1]$$

Here, R is the neuron's response, D is its net excitatory drive, ν (the "semisaturation constant") determines the rate at which the neuron's response saturates as D increases, S (the "suppressive field") is the pooled activity of multiple neurons including the neuron being normalized, and c is a gain term scaling the suppressive field. The suppressive field is a weighted sum of the excitatory drives across the population: $S = \sum_i w_i D_i$, where D_i is the excitatory drive to the ith neuron and w_i is the corresponding weight (*SI Appendix*). The extent of neuronal pooling (determined by the set of weights, w) in the suppressive field can be thought of as an anatomical property reflecting the lateral connectivity across the population. The suppressive field gain term (c) can be thought of as a physiological property determining the context sensitivity of individual neurons to the neuronal milieu in the sense that it scales how much each neuron's response is influenced by the stimulus-dependent population activity. The dependency of neural activity on ν and c is illustrated in Fig. 2. Note that reducing either of these parameters decreases the strength of the divisive normalization signal (thus increasing the E/I ratio), resulting in higher amplitude responses. Importantly, the denominator, $\nu + c \cdot S$, determines how much the population suppresses a neuron's activity, and thus the balance of excitation to inhibition is reflected in the ratio $D : \nu + c \cdot S$.

Divisive normalization is a widespread neural computation. In primary visual cortex, it was first used to explain why responses saturate as stimulus contrast increases (34). It is also thought to adjust the gain of neural responses to efficiently make use of their dynamic range (15). Divisive normalization further accounts for a number of phenomena in auditory cortex (35), multisensory integration (36), and higher-order processes such as attention (37) and rationality (16). In addition, divisive normalization may be critical for neural circuits to implement marginalization, a type of probabilistic inference that eliminates irrelevant information, so-called "nuisance variables" (38).

To illustrate how divisive normalization affects neural activity, we simulated a population of neurons in primary visual cortex (V1) and compared their response properties before and after divisive normalization. Across the population, the receptive fields varied in retinotopic position (X) and orientation (θ) (Fig. 3*A*). For each model neuron, the excitatory drive $D(X, \theta)$ elicited by a stimulus depends on the position and orientation of the receptive field relative to the stimulus (*SI Appendix*). The excitatory drive is inhibited divisively by a suppressive field $S(X, \theta)$ reflecting the pooled activity of neurons with nearby receptive fields. The strength of the suppressive field, and therefore its inhibitory effect, increases with the excitatory drive as well as the extent of neuronal pooling. The response of each model neuron, indexed by its receptive field position and orientation, is thus described by the following equation:

$$R(X, \theta) = \frac{D(X, \theta)}{\nu + c \cdot S(X, \theta)}. \qquad [2]$$

The effect of divisive normalization on the responses of a model V1 neuron to sinusoidal gratings of different contrasts,

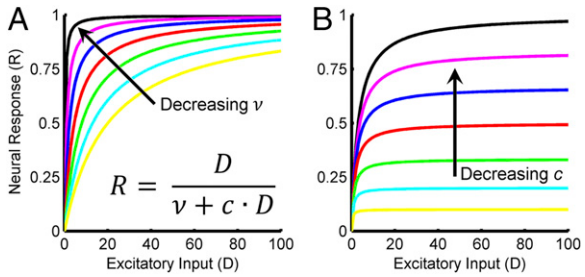


Fig. 2. The effect of divisive normalization parameters ν and c on simulated neural responses. Neural responses (R) are plotted as a function of the excitatory input (D). The equation describing the response functions is shown in *A*. For simplification, the suppressive field is set equal to D. (*A*) Changing the semisaturation constant (ν). Decreasing ν (with constant c) increases the E/I ratio, resulting in responses that saturate at lower values of D. (*B*) Changing the suppressive field gain term (c). Decreasing c (with constant ν) increases the E/I ratio, resulting in an overall increase in response amplitude.

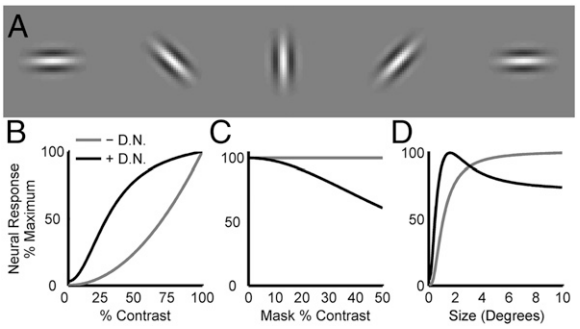


Fig. 3. Effects of divisive normalization on a model of primary visual cortex. (*A*) Receptive fields of five neurons with different retinotopic positions and orientations. (*B*) Contrast response function without (– D.N.) and with (+ D.N.) divisive normalization for a model neuron. The stimuli were gratings of the optimal position, orientation, and size for that neuron. Divisive normalization causes the response to saturate with increasing contrast. (*C*) Cross-orientation suppression in the same neuron. The plot shows responses to stimuli constructed by summing the preferred grating at 50% contrast and an orthogonal grating ("mask") of different contrasts. Without divisive normalization, the response is unaffected by the mask. With divisive normalization, the mask has a suppressive effect that increases with mask contrast. (*D*) Size tuning for the same neuron. Without divisive normalization, the response increases monotonically with stimulus size and saturates. The saturation reflects that the neuron is activated equally well by any stimulus larger than its receptive field. With divisive normalization, the response first increases with stimulus size but then decreases, resulting in a preferred size. The decrease in activity reflects that larger stimuli activate more neurons, thereby increasing the suppressive effect of divisive normalization. (*B–D*) Response amplitudes are inherently smaller with than without divisive normalization. To highlight differences in the shapes of the response functions, each curve is plotted as a percentage of its maximum value.

orientations, and sizes is shown in Fig. 3 *B–D*. Without divisive normalization, the response amplitude grows without bound as the stimulus contrast increases. However, the responses of real V1 neurons saturate with increasing contrast (34), which also occurs in the model with divisive normalization (Fig. 3*B*). Neurons in V1 also display a context sensitivity in which responses to a sinusoidal grating at the preferred orientation are suppressed by the simultaneous presentation of a second grating with an orthogonal orientation. This property of V1 responses is similarly accounted for by divisive normalization (Fig. 3*C*). Surround suppression, which contributes to the size selectivity of V1 neurons (39), can also be explained by divisive normalization. Without divisive normalization, the model responses increase monotonically with stimulus size and saturate. However, with divisive normalization, the behavior is qualitatively different. As the stimulus size increases, the excitatory drive initially outweighs the network inhibition and the response amplitude increases. This occurs until a critical stimulus size determined by $\nu + c \cdot S(X, \theta)$ is reached, at which point the inhibition becomes sufficiently strong to reduce the response amplitude, resulting in a well-defined peak in the size tuning curve (Fig. 3*D*).

Connecting Divisive Normalization and Autism

There are several ways an increased E/I ratio can be modeled using Eq. **2**. One possibility is an increase in excitation, which can be achieved by multiplying the excitatory drive (D) by a number greater than 1. An increase in D could reflect increased glutamate-related excitation, consistent with physiological data on autism (25). An increased E/I ratio could also be due to decreased inhibition, which can be modeled as a decrease in either the semisaturation constant (ν) or the suppressive field gain term (c) (Fig. 2). Decreases in ν or c may reflect decreases in GABA-related inhibition that are also consistent with physiological data on autism (7, 23, 31, 32). Changes in the extent of neuronal pooling in the suppressive field $S(X, \theta)$ (e.g., altered lateral connectivity) could also alter the amount of inhibition acting on a neuron. In particular, reducing the extent of neuronal pooling in the model increases the E/I ratio (*SI Appendix*). Considering the large number of autism susceptibility genes, any or all of these factors may contribute on an individual basis.

Although autism may conceptually affect multiple parameters in Eq. **2**, here we focus on the suppressive field gain term (c), which determines the context sensitivity of the neurons, controlling how much each neuron's responses are influenced by the stimulus-dependent population activity. An increased E/I ratio, as is implicated in autism (9), can be simulated by reducing c, thereby attenuating the inhibitory influence of the neuronal milieu on the activity of individual neurons. Autism can thus be putatively simulated by decreasing c, with the degree of severity increasing as c decreases. In this way, we defined an "autism model" of primary visual cortex in which there is a 25% reduction in c relative to the "typically developing control" model used above (*SI Appendix*). With the exception of this change in the suppressive field gain term, the autism and typically developing control models are identical.

In the following sections, we examine how divisive normalization can account for perceptual consequences of autism by comparing the activity of the autism and typically developing control models. We first present simulations of two psychophysical studies exploring how autism affects performance in simple visual tasks relying heavily on primary visual cortex, thus allowing the studies to be simulated using the V1 models. Interestingly, the same change in the suppressive field gain term (c) qualitatively accounts for the findings of both studies. A third simulation is then performed to show how Bayesian priors can be implemented through divisive normalization, linking alterations in neural computation to high-level hypotheses about how autism affects the ability to make inferences about the world. Last, broader connections between autism and divisive normalization are discussed to link major theories and findings on the disorder to divisive normalization, as well as make predictions about the behavioral consequences of autism.

Simulation 1: Visual Spatial Suppression

Recent studies report that visual spatial suppression, which is linked to divisive normalization (39) (Fig. 3*D*), may be altered in autism (40, 41). In one study, Foss-Feig et al. (40) presented drifting gratings that varied in size and contrast, and had subjects indicate the direction of motion (left vs. right). When the stimuli were presented at high contrast, performance worsened (the time required to judge the direction of motion lengthened) as the size of the stimulus increased for both typically developing controls and subjects with autism. However, subjects with autism performed systematically better than controls across all stimulus sizes. This result is illustrated in Fig. 4*A*, where inverse duration thresholds are plotted such that larger values indicate better performance. For small stimuli presented at low contrast, the performance difference between the groups disappeared (Fig. 4*B*). These results raise two questions: (*i*) what changes in neural computation can account for the findings, and (*ii*) are these changes consistent with the physiology of autism?

Because our model simulates neuronal population activity, answering these questions requires a consideration of how this activity can translate into behavior. One possibility is that population activity is decoded to determine the most probable stimulus, and the appropriate behavioral response is then selected accordingly (17, 38, 42). This strategy captures the intuition that greater activity in a subpopulation of neurons with similar response properties leads to greater certainty about the stimulus (*SI Appendix*). More specifically, the certainty about a presented stimulus increases with the amplitude of the population response, which is called the population gain (*SI Appendix*,

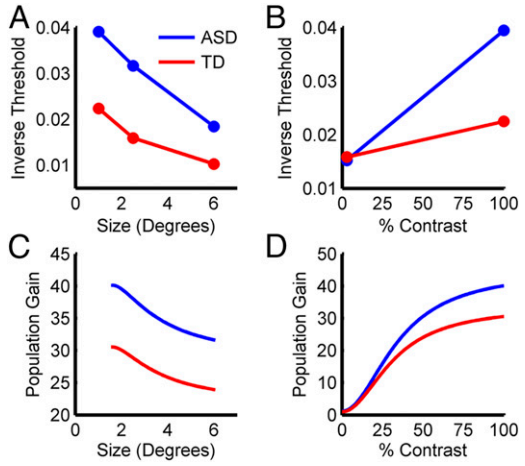


Fig. 4. Simulation 1: visual spatial suppression. (*A*) Psychophysical data showing that the ability to judge direction of motion decreases as stimulus size increases for high contrast stimuli (40). This is true for both typically developing controls (TD; red) and subjects with autism (ASD; blue), but ASD subjects consistently outperform TD subjects. Larger inverse thresholds indicate better performance. (*B*) Psychophysical data showing that for a small stimulus, ASD and TD subjects perform equivalently in judging direction of motion for a low-contrast stimulus, but ASD subjects perform better when the stimulus has a high contrast. (*C*) Simulation results showing population gains for the control (red) and autism (blue) models as a function of stimulus size for high contrast stimuli. The models' responses follow the same pattern as the psychophysical data in *A*. (*D*) Simulation results for the control and autism models as a function of stimulus contrast for small stimuli. The models' responses follow the same pattern as the psychophysical data in *B*.

Fig. S1). A key implication connecting behavior to neural activity is therefore that task performance will be better when the population gain is larger, and worse when that gain is lower. As demonstrated below, larger population gains and thus improved task performance can occur as a consequence of an attenuated divisive normalization signal (increased E/I ratio).

Based on these considerations, the psychophysical findings of Foss-Feig et al. (40) imply several testable predictions about the underlying neural activity. First, spatial suppression should appear as a reduction in the population gain as the stimulus size increases. Second, for subjects with autism to perform better than controls at high contrasts, population gains should be higher in autism. Third, similar task performance at low contrasts predicts that, under these conditions, population gains will be similar for controls and subjects with autism. To test these predictions in silico, we examined the model responses to sinusoidal gratings of different sizes and contrasts. As predicted, the population gains decreased for high-contrast stimuli of increasing size, but were always higher for the autism than the control model (Fig. 4*C*). Moreover, the population gains of the two models were nearly identical for small stimuli at low contrasts, but diverged progressively as the contrast increased (Fig. 4*D*). This result suggests that performance differences between controls and subjects with autism in this task will increase smoothly with stimulus contrast. In addition, the similarity of the population gains at low contrasts may account for why autism does not affect contrast sensitivity (the lowest contrast at which sinusoidal gratings can be reliably detected), since contrast sensitivities are themselves very low (43). Additional simulations examining how changes in the semisaturation constant and the extent of neuronal pooling affect the model responses are shown in *SI Appendix*, Fig. S2. These simulations show that an increased E/I ratio resulting from altered divisive normalization can affect neural computation in a manner that qualitatively predicts perceptual consequences of autism.

An intuition for the results shown in Fig. 4 *C* and *D* can be found by examining Eq. **2**. First consider the finding of similar psychophysical performance at low contrasts, and note that the magnitude of the suppressive field $S(X,\theta)$ is small at low contrasts due to weak stimulus drives. As such, the inhibition from $\nu + c \cdot S(X,\theta)$ is roughly independent of c at low contrasts. In other words, the population activity is not large enough to strongly engage divisive normalization, and so little to no difference is observed between the control and autism models. However, at high contrasts, the magnitude of the suppressive field $S(X,\theta)$ is large enough to strongly engage divisive normalization, allowing different values of the suppressive field gain term to exert differential effects. In particular, the lower value of the suppressive field gain term (c) in the autism compared with the control model results in less inhibition and thus larger population gains at high contrasts, leading to better task performance.

Simulation 2: Tunnel Vision

The visual detection of a target is facilitated by presenting it within close proximity to an attentional cue (44). Recently, Robertson et al. (45) found that, as the distance between the attentional cue and target increases (*SI Appendix*, Fig. S3*A*), the rate at which performance falls off is greater for subjects with autism than typically developing controls, suggesting there is a sharper gradient of attention in autism, or "tunnel vision." This result is illustrated in Fig. 5*A*, where relative performance scores taking into account both reaction time and accuracy are plotted. Larger values indicate faster, more accurate detection. Because the

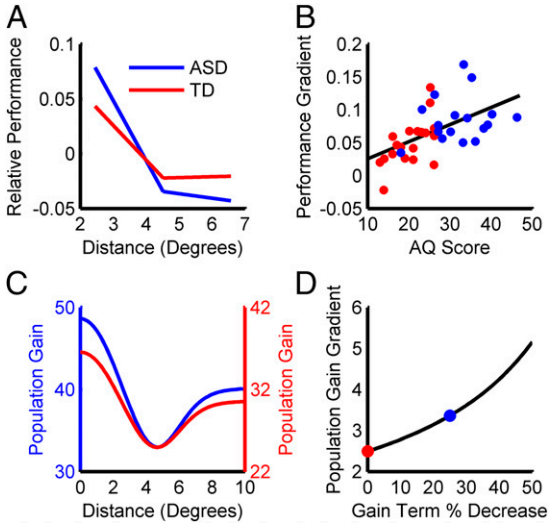


Fig. 5. Simulation 2: tunnel vision. (*A*) Psychophysical data showing that performance worsens as the target distance from the cue increases for both typically developing controls (TD; red) and subjects with autism (ASD; blue). Larger relative performance scores indicate faster, more accurate detection. Note that the rate at which performance decays is greater for ASD than TD subjects (there is greater overall change). (*B*) Psychophysical data showing that the performance gradient increases with the degree of autism symptomatology assessed using the autism spectrum quotient (AQ). ASD subjects (blue points) were identified based on Autism Diagnostic Observation Schedule scores. (*C*) Simulation results showing population gains for the control (red) and autism (blue) models as a function of target distance from the cue. The models' responses follow the same pattern as the psychophysical data in *A* and further reproduce the nonmonotonic shape of the attentional field (44). To highlight the gradient difference between the control and autism models, the *y* axes are shifted to align the troughs of the curves. (*D*) Simulation results showing that, as the suppressive field gain term decreases (simulating an increasing degree of autism symptomatology), the gradient of the population gain increases, consistent with the psychophysical data in *B*. The colored dots correspond to the control and autism models in *C*.

stimuli were tailored to each subject to match baseline task difficulty, and the subject-averaged performance scores were mean subtracted separately for the control and autism groups, only the steepness of the gradient can be compared across groups. Interestingly, the study found that the steepness of the attention gradient was correlated with the degree of autism symptomatology (Fig. 5*B*). Here, we show that the same alteration in divisive normalization that accounts for the findings of Foss-Feig et al. (40) can qualitatively account for these results.

For this simulation, an attentional field $A(X)$ was incorporated to define an attention-modulated excitatory drive: $D_A(X,\theta) = A(X) \cdot D(X,\theta)$ (37) (*SI Appendix*). The parameters of the attentional field were the same for the control and autism models, and with the exception of introducing the attentional field, all aspects were the same as in the previous simulation. The attentional field also affects the divisive normalization signal as a consequence of neuronal pooling in the suppressive field, $S_A(X,\theta)$. Incorporating the effects of attention, the response of each model neuron is described by the following equation:

$$R(X,\theta) = \frac{D_A(X,\theta)}{\nu + c \cdot S_A(X,\theta)}. \quad [3]$$

To examine the effect of the attentional field on the model responses, sinusoidal gratings were presented at different distances from the center of the attentional field, and the population gain at those locations measured. Recall that better task performance is achieved when the population gain is larger (*SI Appendix*, Fig. S1). Consistent with the findings of Robertson et al. (45), the population gain decreased for both models as the distance between the target and attentional cue increased, with faster falloff in the autism model (Fig. 5*C*). Moreover, as we increased the simulated degree of autism symptomatology by further decreasing the suppressive field gain term, the rate at which the population gain fell off increased (Fig. 5*D*).

These results reflect an interaction between the attentional field and divisive normalization. The existence of the gradient in the population gain is due to the attentional field, but the steepness depends on the strength of the divisive normalization signal. The gradient arises because the attentional field produces a location-dependent increase in the strength of the excitatory drive, $D_A(X,\theta)$. This effect is balanced by inhibition from the suppressive field, $S_A(X,\theta)$, with the magnitude of the divisive normalization signal depending on the suppressive field gain term (c). Because the smaller value of c in the autism model results in less inhibition, the attentional field has a larger effect that gives rise to a sharper gradient in the population gain. We additionally found that the lower value of c in the autism model resulted in larger population gains (implying better task performance) at the largest target distances where the attentional field has little effect (Fig. 5*C*). We therefore ran a second simulation at a reduced contrast, such that the population gains for the control and autism models were approximately matched at large target distances (*SI Appendix*, Fig. S3*B*). This manipulation is similar to the measures Robertson et al. (45) took to match baseline task difficulty across subjects. Importantly, under this condition, the modeling results remained consistent with the psychophysical findings; namely, a steeper gradient in the population gain for the autism than the control model, which increased as the suppressive field gain term decreased (*SI Appendix*, Fig. S3*C*). Additional simulations examining how changes in the extent of neuronal pooling and the semisaturation constant affect the model responses are shown in *SI Appendix*, Fig. S3 *D* and *E*. It is further interesting to note that our results may explain the apparent conflict between the study by Robertson et al. (45) and another recent study suggesting that exogenous spatial attention may not be affected in autism (46). Specifically, because the attentional field was the same for the control and autism models, the differences in their responses were entirely due to the difference in their suppressive field gain terms. This result indicates that a sharper gradient of attention in autism may reflect altered divisive normalization rather than a change in attentional mechanisms.

Simulation 3: Neural Implementation of Bayesian Priors

Several papers have suggested that autism impairs the ability to perform statistical inference about the sensory environment (18–20), reducing the influence of past experience on the interpretation of current sensory information. Although this hypothesis can be formulated in several ways, the Bayesian framework provides an intuitive approach, describing how incoming sensory information is combined with past experience to infer the most likely stimulus. In particular, attenuation of the Bayesian prior (the collected representation of past experience) in autism would reduce the influence of past experience on the interpretation of current sensory information (19). To the extent that a Bayesian prior accurately reflects the statistics of the world, it will improve task performance by reducing the number of probable stimuli. As such, an attenuated prior in autism could potentially increase behavioral sensitivity to sensory noise, as well as increase variability in stimulus-driven neural activity, both of which are consistent with recent findings on the disorder (47, 48). We next simulate how Bayesian priors can be implemented through divisive normalization, establishing a link between alterations in neural computation and high-level hypotheses about how autism affects the ability to perform statistical inference.

In the model, experience modifies the strength of lateral connectivity across the population, transforming the suppressive field gain term (c) from a constant into a function of the neuronal tuning properties (49) (*SI Appendix*, Fig. S4*A*). In this way, a prior turns stimulus-driven responses into a reflection of both current sensory information and past experience. As an example, we modeled the "oblique effect," which describes that humans are most visually sensitive to vertically and horizontally orientated contours (50), presumably reflecting that cardinal orientations are more frequent in natural scenes than oblique orientations (51). For the oblique effect, the prior facilitates responses to cardinal orientations and attenuates responses to oblique orientations (*SI Appendix*, Fig. S4*B*). Decoding the population activity to discriminate changes in stimulus orientation reveals the effect of the prior; namely, greater sensitivity to cardinal than oblique orientations (*SI Appendix*, Fig. S5). The weaker the prior, the less performance depends on the orientation of the stimulus (*SI Appendix*, Fig. S4*C*). An attenuation of Bayesian priors thus correctly predicts reduced differences in sensitivity to cardinal and oblique orientations in autism (52).

How can divisive normalization account for the proposed attenuation of Bayesian priors in autism (19)? One possibility is that a reduction in the suppressive field gain term (c; as in the first two simulations) attenuates the influence of the population on individual neurons, thereby reducing the effect of priors. The extent to which experience modifies c could also be attenuated, such that a given level of experience produces smaller changes in c for individuals with autism than typically developing peers. In other words, plasticity in the strength of experience-dependent lateral connectivity may be diminished in the disorder. This possibility is consistent with the observation that many autism susceptibility genes code for synaptic proteins or control synaptic development and function, suggesting that the effect of experience on synapses is altered in autism (53).

Local vs. Global Processing

Compared to typically developing peers, individuals with autism are thought to have a bias toward the processing of "local" stimulus features (54–57). The hierarchical figures test, in which

local features are used to define a global feature, provides an illustrative example. Consider a local feature, the letter "A" reproduced many times in a small font size and arranged to create a large letter "F," the global feature. When the task is to report if a particular letter is present, subjects with autism make fewer errors if the letter is the local feature than if it is the global feature, whereas controls make fewer errors if the letter is the global feature (55). When the letter of interest is the global feature, the local feature is a nuisance variable in the sense that it makes no difference if it is the letter "A" or any other letter. The elimination of nuisance variables is called marginalization, and theoretical work suggests that the neural implementation of this process requires divisive normalization (38). A bias toward local feature processing in autism is therefore consistent with the possibility of impaired marginalization through altered divisive normalization. More generally, behaviors requiring marginalization such as social cognition (58), visual search (59), reference frame transformations (60), and causal inference (38), may be altered in autism. Consistent with this prediction, impaired social cognition is a diagnostic criterion for autism, visual search is altered in the disorder (61), and an increased egocentric perspective in autism (62) may reflect an impairment in reference frame transformations.

Simple vs. Complex Stimuli

Individuals with autism are often reported to perform better at tasks involving "simple" stimuli, whereas typically developing controls may be better at tasks involving "complex" stimuli (63, 64). For example, in the auditory system, enhanced performance is reported in autism when a discrimination task is performed using pure tones, but no difference or deficits are observed when the stimuli are more complex (65–67). Consider that the amount of processing, and thus the number of processing stages (e.g., hierarchically organized brain regions), required to analyze sensory information is linked to the complexity of the stimulus. For example, contour orientation is readily decoded from V1 (68), but decoding object identity is accomplished in higher stages of cortex (69). Theoretical work shows that, for biologically realistic, hierarchical neural network models to perform complex tasks such as object identification accurately, it is critical to include divisive normalization-like computations at every processing stage (70, 71). If divisive normalization is altered beyond the early stages of sensory processing in autism, then it could result in impaired processing specifically for complex, but not simple, stimuli. Such a deficit would be particularly detrimental when local features must be combined to form a complex whole and may therefore account for impaired face processing in autism, which appears to reflect a more feature-based analysis and reduced use of contextual information in creating face composites (72). Indeed, the importance of divisive normalization in performing hierarchical processing may create a trade-off in the ability to perform tasks requiring fewer vs. more levels of processing, such that an overall decrease in the strength of divisive normalization signals would not be globally beneficial.

Multisensory Processing

Altered multisensory processing, for example, in the integration of visual and auditory signals, is reported by some autism studies (73–75). However, it is unclear whether these results reflect differences in earlier unisensory representations or in the process of multisensory integration itself. The possibility of intact multisensory processing is supported by a recent study reporting near-optimal integration of visual and vestibular cues in self-motion perception in both controls and subjects with autism (48). Importantly, this finding is not inconsistent with the hypothesis of altered divisive normalization in autism since cue integration does not theoretically require divisive normalization (42). Altered divisive normalization in autism does, however, predict changes in other forms of multisensory processing that require divisive normalization, such as cue conflict conditions and causal inference (36, 38).

Rationality

Rational behavior in value-based decision tasks implies that choices should reflect the context-independent values of available options. In other words, choices about an option should depend neither on the quantity/quality of other options, nor on how the option is framed (e.g., in terms of gain vs. loss). However, individuals are often irrational, making value-based decisions that show context dependence. As discussed above, divisive normalization makes neurons context sensitive; for example, resulting in cross-orientation suppression (Fig. 3*C*). In an analogous manner, divisive normalization acting on a population of neurons encoding the value of available options in a decision task can account for the context dependence, and therefore irrationality, of value-based decisions (16). In such a population, the suppressive field represents the overall value of available options, and divisive normalization transforms an absolute value representation into a relative representation that depends on the context of available choices. Divisive normalization can thus contribute to context-dependent violations of rationality in which the suppressive field gain term is particularly important because it scales how much each option's value is influenced by other options. It is therefore intriguing to speculate that a decrease in the suppressive field gain term in autism can result in reduced contextual sensitivity in value-based decisions. Consistent with this prediction, enhanced logical consistency in value-based decisions is observed in autism as a consequence of reduced susceptibility to contextual framing (76).

Conclusions

A problem currently faced in autism research is that the disorder is both genetically heterogeneous and phenotypically diverse. Here, we examined how computational models of nonlinear neural circuits can bridge levels of analysis, connecting genetic and molecular findings supporting an increased E/I ratio in autism to perceptual data on the disorder. In particular, we showed that a reduction in the amount of inhibition occurring through divisive normalization can account for perceptual consequences of autism. Interestingly, our simulations implicate the context-dependent neuronal milieu as having a critical role in autism, such that the less influence the population has on the activity of individual neurons, the more severe the degree of autism symptomatology. Importantly, computational frameworks such as presented here can provide a systematic mechanism for generating falsifiable hypotheses about the neural basis of autism. For example, altered divisive normalization in autism predicts that the disorder will broadly affect processes requiring marginalization (38), such as social cognition (58) and visual search (59).

The phenotypic diversity of autism may in part reflect that the neural mechanisms implementing divisive normalization differ across brain regions (15). Our results thus predict that the behavioral consequences of autism will vary across individuals, depending qualitatively and quantitatively on where and how the disorder impacts divisive normalization. Qualitative differences between individuals should occur when alterations in divisive normalization impact different brain areas. Quantitative differences should instead reflect the extent to which divisive normalization is affected; for example, the percent reduction in the suppressive field gain term (Fig. 5*D*). Supporting this idea, the GABAergic pathways likely contribute to autism (7, 8, 31, 32), and $GABA_A$ and $GABA_B$ can contribute differently to divisive normalization. In V1, $GABA_A$ modulates response gain but not contrast sensitivity (77), suggesting it contributes to the suppressive field gain term (c) but not the semisaturation constant (ν). In

the auditory system, $GABA_B$ is implicated in both response gain and sensitivity, suggesting it may contribute to c as well as ν (78).

Here, we focused on how reducing c can account for perceptual consequences of autism, including phenotypic diversity within the same task. A reduction in c is consistent with reduced $GABA_A$ inhibition in V1 (77), and our results correspondingly predict higher average V1 firing rates in autism than controls. Given the statistical properties of spiking neural activity (79), this result also predicts greater trial-by-trial response variability in autism. Evidence supporting these predictions comes from imaging studies reporting larger stimulus-driven response amplitudes (80) or increased variance (47) in autism, as well as recent psychophysical findings (81). In one imaging study, increased stimulus-driven activity in auditory cortex associated with low-level feature processing was observed in subjects with autism compared to typically developing controls (82). Interestingly, this finding was specific to subjects with autism showing speech onset delay, a subgroup for which enhanced performance on low-level auditory tasks such as pitch discrimination may be specific (67). A reduction in c is also consistent with the finding that contrast sensitivity is not affected in autism (43), which would have otherwise suggested a change in ν (Fig. 2*A*). Although normal contrast sensitivity is consistent with intact gain control, it is possible that sensory hypersensitivity in autism (83) reflects gain control deficits. It is thus interesting to speculate that steady-state values of ν are not altered in autism, but the temporal process by which ν changes based on sensory stimulation is impaired (20). In addition, a reduction in c could affect neural decoding by reducing noise correlations between neurons (84), or decreasing the efficiency of simple decoders (85), both of which are potential consequences of a reduced influence of the neuronal milieu on the activity of single cells.

Divisive normalization parameters other than c may also contribute to the phenotypic diversity of autism. This possibility was explored by examining the effects of changing the extent of neuronal pooling and ν (*SI Appendix*, Figs. S2 and S3). For the spatial suppression simulation, results similar to changing c (Fig. 4) were achieved by decreasing the extent of neuronal pooling (increasing the E/I ratio), but the effects were weaker. Moreover, as the size of the stimulus increased, there was a reduction in the rate of spatial suppression (*SI Appendix*, Fig. S2) that appears inconsistent with the psychophysical data (40). A decrease in ν (increasing the E/I ratio) also produced similar spatial suppression results, but the effects were highly attenuated and would alter contrast sensitivity, inconsistent with previous findings (43). For the tunnel vision simulation (Fig. 5), sharper gradients of attention resulted from increases in the extent of neuronal pooling or ν (*SI Appendix*, Fig. S3), decreasing the E/I ratio. Changes in these parameters thus provide a less parsimonious explanation for the autism symptomatology explored here than a change in c, because they needed to be in opposite directions for the two sets of psychophysical findings. Importantly, this observation does not imply that these parameters are unaffected in autism; in fact, their diverse effects may contribute to the disorder's phenotypic diversity. By considering where in the brain and how much these parameters are affected, it may be possible to account for a wide array of behavioral data on autism. Although we focused on how divisive normalization can account for psychophysical findings in simple tasks relying heavily on a single brain area, it will be important for future computational work to investigate how autism affects complex functions (e.g., face processing) involving multiple brain areas. Such work will call for hierarchical, multilayered networks in which divisive normalization is essential (70, 71), and may provide insights into the finding of decreased functional connectivity across brain areas in autism (86–89). Indeed, a recent study implicates divisive normalization in cross-area information coupling (90), suggesting that altered functional connectivity in autism may be partly attributable to divisive normalization.

The computational framework described in this study provides a formalism for investigating how alterations in neural computation may give rise to autism symptomatology. Adaptations of this approach may provide insights into other mental health disorders such as schizophrenia (10, 91, 92), and perhaps some aspects of aging (93). The results of our simulations further suggest that behavioral assays combined with computational modeling may be useful in identifying altered physiological pathways in individuals, and thus in facilitating the development of individualized treatment plans. We suggest that computational perspectives can play an important role in the future of mental health research, providing insights that will aid in understanding and treating complex disorders such as autism.

ACKNOWLEDGMENTS. We thank Ryan Ash, Reuben Fan, Eliana Klier, Xaq Pitkow, Adhira Sunkara, and Mingshan Xue for comments. This work was supported by Integrative Graduate Education and Research Traineeship Training Grant 43413-I (to J.S.P.) and Simons Foundation Autism Research Initiative 247992 (to D.E.A.).

1. Wing L, Gould J (1979) Severe impairments of social interaction and associated abnormalities in children: Epidemiology and classification. *J Autism Dev Disord* 9(1):11–29.
2. Newschaffer CJ, Falb MD, Gurney JG (2005) National autism prevalence trends from United States special education data. *Pediatrics* 115(3):e277–e282.
3. Autism and Developmental Disabilities Monitoring Network Surveillance Year 2000 Principal Investigators; Centers for Disease Control and Prevention (2007) Prevalence of autism spectrum disorders: Autism and developmental disabilities monitoring network, six sites, United States, 2000. *MMWR Surveill Summ* 56(1):1–11.
4. Developmental Disabilities Monitoring Network Surveillance Year 2010 Principal Investigators; Centers for Disease Control and Prevention (2014) Prevalence of autism spectrum disorders among children aged 8 years: Autism and developmental disabilities monitoring network, 11 sites, United States, 2010. *MMWR Surveill Summ* 63(2):1–21.
5. Ronemus M, Iossifov I, Levy D, Wigler M (2014) The role of de novo mutations in the genetics of autism spectrum disorders. *Nat Rev Genet* 15(2):133–141.
6. Walsh CA, Morrow EM, Rubenstein JL (2008) Autism and brain development. *Cell* 135(3):396–400.
7. Chao HT, et al. (2010) Dysfunction in GABA signalling mediates autism-like stereotypies and Rett syndrome phenotypes. *Nature* 468(7321):263–269.
8. Han S, Tai C, Jones CJ, Scheuer T, Catterall WA (2014) Enhancement of inhibitory neurotransmission by $GABA_A$ receptors having $\alpha_{2,3}$-subunits ameliorates behavioral deficits in a mouse model of autism. *Neuron* 81(6):1282–1289.
9. Rubenstein JL, Merzenich MM (2003) Model of autism: Increased ratio of excitation/inhibition in key neural systems. *Genes Brain Behav* 2(5):255–267.
10. Yizhar O, et al. (2011) Neocortical excitation/inhibition balance in information processing and social dysfunction. *Nature* 477(7363):171–178.
11. Freitag CM, Kleser C, Schneider M, von Gontard A (2007) Quantitative assessment of neuromotor function in adolescents with high functioning autism and Asperger Syndrome. *J Autism Dev Disord* 37(5):948–959.
12. Gabriels RL, et al. (2008) Is there a relationship between restricted, repetitive, stereotyped behaviors and interests and abnormal sensory response in children with autism spectrum disorders? *Res Autism Spectr Disord* 2(4):660–670.
13. Haswell CC, Izawa J, Dowell LR, Mostofsky SH, Shadmehr R (2009) Representation of internal models of action in the autistic brain. *Nat Neurosci* 12(8):970–972.
14. Marko MK, et al. (2015) Behavioural and neural basis of anomalous motor learning in children with autism. *Brain* 138(Pt 3):784–797.
15. Carandini M, Heeger DJ (2012) Normalization as a canonical neural computation. *Nat Rev Neurosci* 13(1):51–62.
16. Louie K, Khaw MW, Glimcher PW (2013) Normalization is a general neural mechanism for context-dependent decision making. *Proc Natl Acad Sci USA* 110(15):6139–6144.
17. Seilheimer RL, Rosenberg A, Angelaki DE (2014) Models and processes of multisensory cue combination. *Curr Opin Neurobiol* 25:38–46.
18. Qian N, Lipkin RM (2011) A learning-style theory for understanding autistic behaviors. *Front Hum Neurosci* 5:77.
19. Pellicano E, Burr D (2012) When the world becomes "too real": A Bayesian explanation of autistic perception. *Trends Cogn Sci* 16(10):504–510.
20. Sinha P, et al. (2014) Autism as a disorder of prediction. *Proc Natl Acad Sci USA* 111(42):15220–15225.
21. Hensch TK (2005) Critical period plasticity in local cortical circuits. *Nat Rev Neurosci* 6(11):877–888.
22. Fagiolini M, Hensch TK (2000) Inhibitory threshold for critical-period activation in primary visual cortex. *Nature* 404(6774):183–186.
23. Hensch TK, et al. (1998) Local GABA circuit control of experience-dependent plasticity in developing visual cortex. *Science* 282(5393):1504–1508.

24. Volkmar FR, Nelson DS (1990) Seizure disorders in autism. *J Am Acad Child Adolesc Psychiatry* 29(1):127–129.
25. Shinohe A, et al. (2006) Increased serum levels of glutamate in adult patients with autism. *Prog Neuropsychopharmacol Biol Psychiatry* 30(8):1472–1477.
26. Fatemi SH, et al. (2014) Downregulation of $GABA_A$ receptor protein subunits α6, β2, δ, ε, γ2, θ, and ρ2 in superior frontal cortex of subjects with autism. *J Autism Dev Disord* 44(8):1833–1845.
27. Jamain S, et al.; Paris Autism Research International Sibpair (PARIS) Study (2002) Linkage and association of the glutamate receptor 6 gene with autism. *Mol Psychiatry* 7(3):302–310.
28. Cook EH, Jr, et al. (1998) Linkage-disequilibrium mapping of autistic disorder, with 15q11-13 markers. *Am J Hum Genet* 62(5):1077–1083.
29. Fatemi SH, Reutiman TJ, Folsom TD, Thuras PD (2009) $GABA_A$ receptor downregulation in brains of subjects with autism. *J Autism Dev Disord* 39(2):223–230.
30. Fatemi SH, Folsom TD, Reutiman TJ, Thuras PD (2009) Expression of $GABA_B$ receptors is altered in brains of subjects with autism. *Cerebellum* 8(1):64–69.
31. Yip J, Soghomonian JJ, Blatt GJ (2007) Decreased GAD67 mRNA levels in cerebellar Purkinje cells in autism: Pathophysiological implications. *Acta Neuropathol* 113(5): 559–568.
32. Yip J, Soghomonian JJ, Blatt GJ (2009) Decreased GAD65 mRNA levels in select subpopulations of neurons in the cerebellar dentate nuclei in autism: An in situ hybridization study. *Autism Res* 2(1):50–59.
33. Gkogkas CG, et al. (2013) Autism-related deficits via dysregulated eIF4E-dependent translational control. *Nature* 493(7432):371–377.
34. Heeger DJ (1992) Normalization of cell responses in cat striate cortex. *Vis Neurosci* 9(2):181–197.
35. Rabinowitz NC, Willmore BD, Schnupp JW, King AJ (2011) Contrast gain control in auditory cortex. *Neuron* 70(6):1178–1191.
36. Ohshiro T, Angelaki DE, DeAngelis GC (2011) A normalization model of multisensory integration. *Nat Neurosci* 14(6):775–782.
37. Reynolds JH, Heeger DJ (2009) The normalization model of attention. *Neuron* 61(2): 168–185.
38. Beck JM, Latham PE, Pouget A (2011) Marginalization in neural circuits with divisive normalization. *J Neurosci* 31(43):15310–15319.
39. Sceniak MP, Hawken MJ, Shapley R (2001) Visual spatial characterization of macaque V1 neurons. *J Neurophysiol* 85(5):1873–1887.
40. Foss-Feig JH, Tadin D, Schauder KB, Cascio CJ (2013) A substantial and unexpected enhancement of motion perception in autism. *J Neurosci* 33(19):8243–8249.
41. Flevaris AV, Murray SO (2014) Orientation-specific surround suppression in the primary visual cortex varies as a function of autistic tendency. *Front Hum Neurosci* 8:1017.
42. Ma WJ, Beck JM, Latham PE, Pouget A (2006) Bayesian inference with probabilistic population codes. *Nat Neurosci* 9(11):1432–1438.
43. Koh HC, Milne E, Dobkins K (2010) Spatial contrast sensitivity in adolescents with autism spectrum disorders. *J Autism Dev Disord* 40(8):978–987.
44. Müller NG, Mollenhauer M, Rösler A, Kleinschmidt A (2005) The attentional field has a Mexican hat distribution. *Vision Res* 45(9):1129–1137.
45. Robertson CE, Kravitz DJ, Freyberg J, Baron-Cohen S, Baker CI (2013) Tunnel vision: Sharper gradient of spatial attention in autism. *J Neurosci* 33(16):6776–6781.
46. Grubb MA, et al. (2013) Exogenous spatial attention: Evidence for intact functioning in adults with autism spectrum disorder. *J Vis* 13(14):9.
47. Dinstein I, et al. (2012) Unreliable evoked responses in autism. *Neuron* 75(6):981–991.
48. Zaidel A, Goin-Kochel RP, Angelaki DE (2015) Self-motion perception in autism is compromised by visual noise but integrated optimally across multiple senses. *Proc Natl Acad Sci USA* 112(20):6461–6466.
49. Schwartz O, Coen-Cagli R (2013) Visual attention and flexible normalization pools. *J Vis* 13(1):25.
50. Westheimer G, Beard BL (1998) Orientation dependency for foveal line stimuli: Detection and intensity discrimination, resolution, orientation discrimination and Vernier acuity. *Vision Res* 38(8):1097–1103.
51. Coppola DM, Purves HR, McCoy AN, Purves D (1998) The distribution of oriented contours in the real world. *Proc Natl Acad Sci USA* 95(7):4002–4006.
52. Dickinson A, Jones M, Milne E (2014) Oblique orientation discrimination thresholds are superior in those with a high level of autistic traits. *J Autism Dev Disord* 44(11): 2844–2850.
53. Ebert DH, Greenberg ME (2013) Activity-dependent neuronal signalling and autism spectrum disorder. *Nature* 493(7432):327–337.
54. Mottron L, Belleville S, Ménard E (1999) Local bias in autistic subjects as evidenced by graphic tasks: Perceptual hierarchization or working memory deficit? *J Child Psychol Psychiatry* 40(5):743–755.
55. Plaisted K, Swettenham J, Rees L (1999) Children with autism show local precedence in a divided attention task and global precedence in a selective attention task. *J Child Psychol Psychiatry* 40(5):733–742.
56. Mottron L, Burack JA, Iarocci G, Belleville S, Enns JT (2003) Locally oriented perception with intact global processing among adolescents with high-functioning autism: Evidence from multiple paradigms. *J Child Psychol Psychiatry* 44(6):904–913.
57. Dakin S, Frith U (2005) Vagaries of visual perception in autism. *Neuron* 48(3):497–507.
58. Baker CL, Saxe R, Tenenbaum JB (2009) Action understanding as inverse planning. *Cognition* 113(3):329–349.
59. Mazyar H, van den Berg R, Seilheimer RL, Ma WJ (2013) Independence is elusive: Set size effects on encoding precision in visual search. *J Vis* 13(5):8.
60. Rosenberg A, Angelaki DE (2014) Gravity influences the visual representation of object tilt in parietal cortex. *J Neurosci* 34(43):14170–14180.
61. O'Riordan MA, Plaisted KC, Driver J, Baron-Cohen S (2001) Superior visual search in autism. *J Exp Psychol Hum Percept Perform* 27(3):719–730.
62. Begeer S, Bernstein DM, van Wijhe J, Scheeren AM, Koot HM (2012) A continuous false belief task reveals egocentric biases in children and adolescents with autism spectrum disorders. *Autism* 16(4):357–366.
63. Bertone A, Mottron L, Jelenic P, Faubert J (2003) Motion perception in autism: A "complex" issue. *J Cogn Neurosci* 15(2):218–225.
64. Bertone A, Mottron L, Jelenic P, Faubert J (2005) Enhanced and diminished visuo-spatial information processing in autism depends on stimulus complexity. *Brain* 128(10):2430–2441.
65. Bonnel A, et al. (2003) Enhanced pitch sensitivity in individuals with autism: A signal detection analysis. *J Cogn Neurosci* 15(2):226–235.
66. Russo NM, et al. (2008) Deficient brainstem encoding of pitch in children with autism spectrum disorders. *Clin Neurophysiol* 119(8):1720–1731.
67. Bonnel A, et al. (2010) Enhanced pure-tone pitch discrimination among persons with autism but not Asperger syndrome. *Neuropsychologia* 48(9):2465–2475.
68. Graf AB, Kohn A, Jazayeri M, Movshon JA (2011) Decoding the activity of neuronal populations in macaque primary visual cortex. *Nat Neurosci* 14(2):239–245.
69. Hung CP, Kreiman G, Poggio T, DiCarlo JJ (2005) Fast readout of object identity from macaque inferior temporal cortex. *Science* 310(5749):863–866.
70. Kouh M, Poggio T (2008) A canonical neural circuit for cortical nonlinear operations. *Neural Comput* 20(6):1427–1451.
71. Jarrett K, Kavukcuoglu K, Ranzato M, LeCun Y (2009) What is the best multi-stage architecture for object recognition? *2009 IEEE 12th International Conference on Computer Vision* (IEEE, Piscataway, NJ), pp 2146–2153.
72. Teunisse JP, de Gelder B (2003) Face processing in adolescents with autistic disorder: The inversion and composite effects. *Brain Cogn* 52(3):285–294.
73. Brandwein AB, et al. (2013) The development of multisensory integration in high-functioning autism: High-density electrical mapping and psychophysical measures reveal impairments in the processing of audiovisual inputs. *Cereb Cortex* 23(6): 1329–1341.
74. Collignon O, et al. (2013) Reduced multisensory facilitation in persons with autism. *Cortex* 49(6):1704–1710.
75. Foxe JJ, et al. (2015) Severe multisensory speech integration deficits in high-functioning school-aged children with autism spectrum disorder (ASD) and their resolution during early adolescence. *Cereb Cortex* 25(2):298–312.
76. De Martino B, Harrison NA, Knafo S, Bird G, Dolan RJ (2008) Explaining enhanced logical consistency during decision making in autism. *J Neurosci* 28(42):10746–10750.
77. Katzner S, Busse L, Carandini M (2011) $GABA_A$ inhibition controls response gain in visual cortex. *J Neurosci* 31(16):5931–5941.
78. Magnusson AK, Park TJ, Pecka M, Grothe B, Koch U (2008) Retrograde GABA signaling adjusts sound localization by balancing excitation and inhibition in the brainstem. *Neuron* 59(1):125–137.
79. Gur M, Beylin A, Snodderly DM (1997) Response variability of neurons in primary visual cortex (V1) of alert monkeys. *J Neurosci* 17(8):2914–2920.
80. Schwarzkopf DS, Anderson EJ, de Haas B, White SJ, Rees G (2014) Larger extrastriate population receptive fields in autism spectrum disorders. *J Neurosci* 34(7):2713–2724.
81. Haigh SM, Minshew N, Heeger DJ, Dinstein I, Behrmann M (2015) Over-responsiveness and greater variability in roughness perception in autism. *Autism Res*, 10.1002/aur.1505.
82. Samson F, Zeffiro TA, Doyon J, Benali H, Mottron L (2015) Speech acquisition predicts regions of enhanced cortical response to auditory stimulation in autism spectrum individuals. *J Psychiatr Res*, 10.1016/j.psychires.2015.05.011.
83. Tomchek SD, Dunn W (2007) Sensory processing in children with and without autism: A comparative study using the short sensory profile. *Am J Occup Ther* 61(2):190–200.
84. Averbeck BB, Latham PE, Pouget A (2006) Neural correlations, population coding and computation. *Nat Rev Neurosci* 7(5):358–366.
85. Olsen SR, Bhandawat V, Wilson RI (2010) Divisive normalization in olfactory population codes. *Neuron* 66(2):287–299.
86. Belmonte MK, et al. (2004) Autism and abnormal development of brain connectivity. *J Neurosci* 24(42):9228–9231.
87. Just MA, Cherkassky VL, Keller TA, Kana RK, Minshew NJ (2007) Functional and anatomical cortical underconnectivity in autism: Evidence from an FMRI study of an executive function task and corpus callosum morphometry. *Cereb Cortex* 17(4): 951–961.
88. Schipul SE, Keller TA, Just MA (2011) Inter-regional brain communication and its disturbance in autism. *Front Syst Neurosci* 5:10.
89. Wass S (2011) Distortions and disconnections: Disrupted brain connectivity in autism. *Brain Cogn* 75(1):18–28.
90. Saproo S, Serences JT (2014) Attention improves transfer of motion information between V1 and MT. *J Neurosci* 34(10):3586–3596.
91. Yoon JH, et al. (2010) GABA concentration is reduced in visual cortex in schizophrenia and correlates with orientation-specific surround suppression. *J Neurosci* 30(10): 3777–3781.
92. Tibber MS, et al. (2013) Visual surround suppression in schizophrenia. *Front Psychol* 4:88.
93. Betts LR, Taylor CP, Sekuler AB, Bennett PJ (2005) Aging reduces center-surround antagonism in visual motion processing. *Neuron* 45(3):361–366.

A computational perspective on autism

Ari Rosenberg[*], Jaclyn Sky Patterson, & Dora E. Angelaki[†]

Department of Neuroscience, Baylor College of Medicine, Houston, TX 77030
Email: [*]ari.rosenberg@wisc.edu, [†]angelaki@bcm.edu

SI APPENDIX

Neural Network Model. To simulate the activity of primary visual cortex (V1), we implemented a two-layer neural network performing an energy computation (1-3) followed by divisive normalization (4-6). The first layer consists of two sets of model simple cells with Gabor spatial receptive fields, one set sine-phased (F_s) and the other cosine-phased (F_c). Example simple cell receptive fields are shown in Fig. 3A. The receptive field of a sine-phased simple cell is defined by the equation

$$F_s(X,\theta) = e^{-\frac{X_\theta^2}{2\sigma_x^2}-\frac{Y_\theta^2}{2\sigma_y^2}} \cdot \sin(\mathrm{SF} \cdot X_\theta). \quad [1]$$

Here, $X = (x, y)$ with x and y denoting the horizontal and vertical dimensions of retinotopic space (degrees), $X_\theta = \cos(\theta) \cdot (x - x_0) + \sin(\theta) \cdot (y - y_0)$ and $Y_\theta = -\sin(\theta) \cdot (x - x_0) + \cos(\theta) \cdot (y - y_0)$ where x_0 and y_0 determine the horizontal and vertical positions of the receptive field, σ_x and σ_y set the width and length of the receptive field, θ specifies its orientation, and SF is its spatial frequency (cycles/degree; cyc/°). The receptive field of a cosine-phased simple cell is defined analogously. In the simulations, $\sigma_X = 0.7°, \sigma_Y = 1.2°$, and $\mathrm{SF} = 4$ cyc/°. The receptive field positions vary horizontally between $x_0 = \pm 15°$ spaced every $0.2°$ with the same vertical position ($y_0 = 0°$), and the orientations range between $0° \leq \theta < 180°$ sampled every $1°$. The first layer of the network thus contains 27,180 sine-phased and 27,180 cosine-phased model simple cells.

The second layer of the network consists of a population of complex cells, each of which receives input from one sine-phased and one cosine-phased simple cell with the same retinotopic position and orientation. The stimulus driven excitatory input to each complex cell is given by

$$D(X,\theta) = \mathrm{DC} + [I \cdot F_S(X,\theta)]^2 + [I \cdot F_C(X,\theta)]^2, \quad [2]$$

the sum of a DC offset that introduces a baseline level of activity ($\mathrm{DC} = 2$) and the squared dot products of visual stimulus I and each of the two simple cell receptive fields. The second layer of the network thus contains 27,180 model complex cells.

Divisive normalization was implemented at the second layer of the network, dividing the stimulus driven excitatory input $D(X,\theta)$ to each model complex cell by a measure of the population activity referred to as the suppressive field (7). The suppressive field was calculated by convolving ($\otimes$) a suppressive field kernel describing the extent of neuronal pooling

$$\mathrm{W}(X) = e^{\frac{-\|X\|^2}{2\sigma_S^2}} \quad [3]$$

with the stimulus driven excitatory input $D(X,\theta)$ (7). Note that $\mathrm{W}(X)$ corresponds to the weights in the calculation of the suppressive field discussed in the main text. The parameter σ_S determines the extent of neuronal pooling across receptive field positions, with larger values resulting in greater neuronal pooling. The $\|\cdot\|$ symbol denotes the norm. Due to the falloff in the amplitude of $\mathrm{W}(X)$ with retinotopic distance, neurons with similar receptive field positions have a greater inhibitory effect on each other than neurons with more distal receptive fields. In the simulations, $\sigma_S = \sqrt{5}°$. Because the suppressive field kernel does not depend on orientation (θ is not in the equation), the inhibitory effect of one neuron on another is independent of their orientations (7). The suppressive field kernel $\mathrm{W}(X)$ can be thought of as an anatomical property, determining the spatial extent of

lateral connectivity across the population. It contributes directly to the strength of the divisive normalization signal, with less inhibition occurring when the extent of neuronal pooling is smaller (i.e., if σ_S is smaller). A narrower extent of neuronal pooling therefore results in a larger E/I ratio.

The suppressive field is defined as $S(X,\theta) = \mathrm{W}(X) \otimes D(X,\theta)$. The response of each model complex cell to stimulus I, indexed by its receptive field position (X) and orientation (θ), is then given by the equation

$$R(X,\theta) = \frac{D(X,\theta)}{\nu + c \cdot S(X,\theta)}. \quad [4]$$

As discussed in the main text (Fig. 2), the semisaturation constant (ν) determines how quickly the response of a model neuron saturates as the excitatory drive, $D(X,\theta)$, increases (4, 5). The suppressive field gain term (c) scales the suppressive field, $S(X,\theta)$, and can be thought of as a physiological property, determining the context-sensitivity of the neurons in the sense that it scales how much a neuron's response is influenced by the stimulus-dependent population activity. Note that c sets the amplitude of the suppressive field kernel $\mathrm{W}(X)$. For the simulations presented in Figs. 3, S1, S4, and S5 as well as for the "typically developing control model" in Figs. 4, 5, S2, and S3, the values of these parameters were $\nu = 1$ and $c = 1\text{x}10^{-4}$. In order to increase the E/I ratio, hypothetically simulating autism, a lower value of $c = 7.5\text{x}10^{-5}$ was used with $\nu = 1$ for the "autism model" in Figs. 4, 5, S2, and S3. The phenotypic diversity of autism was modeled in Figs. 5D and S3C by varying c from $1\text{x}10^{-4}$ to $5\text{x}10^{-5}$. In Fig. S2, additional "autism models" were tested with either: (*i*) $\nu = 0.01$ and $c = 1\text{x}10^{-4}$ or (*ii*) $\nu = 1$ and $c = 1\text{x}10^{-4}$ (the control values) but with $\sigma_S = 0.8 \cdot \sqrt{5}°$.

Incorporating Attention. To simulate the effect of attention on neural responses (Figs. 5 and S3), we incorporated an "attentional field" modeled as a Gaussian function over position (7)

$$A(X) = 1 + G_A \cdot e^{-\frac{\|X - X_0\|^2}{2\sigma_A^2}}. \quad [5]$$

The attentional field was centered at $X_0 = (0°, 0°)$ with $G_A = 7$ and $\sigma_A = 2°$. The $\|\cdot\|$ symbol denotes the norm. The strength of the attentional field decreases with distance (X) from the cued location (X_0) but is independent of orientation. The effect of attention was modeled by multiplying the stimulus drive by the attentional field: $D_A(X,\theta) = A(X) \cdot D(X,\theta)$. Because of the DC offset by 1, the attentional field can only facilitate the stimulus drive, $D_A(X,\theta) \geq D(X,\theta)$. In turn, the suppressive field becomes $S_A(X,\theta) = \mathrm{W}(X) \otimes D_A(X,\theta)$, and the equation describing the responses of the model complex cells becomes

$$R(X,\theta) = \frac{D_A(X,\theta)}{\nu + c \cdot S_A(X,\theta)}. \quad [6]$$

The gradient of the population gain (Figs. 5D and S3C) was calculated as the difference between the maximum and minimum population gains divided by the retinotopic distance between their locations.

Incorporating Bayesian Priors. Several papers have suggested that the influence of past experience on the interpretation of current sensory information is impaired in autism (8-10). Here, experience is assumed to shape the activity of individual neurons by modifying the strength of lateral connectivity between neurons in a feature-dependent fashion. The effect of past experience on the neural population was therefore modeled by transforming the suppressive field gain term (c) from a constant into a function of the neurons' tuning properties. As such, experience either: (*i*) decreases inhibition through a feature-dependent decrease in c or (*ii*) increases inhibition through a feature-dependent increase in c. This approach is similar to that taken in a computational study investigating how flexible divisive normalization pools can account for findings on visual attention (11).

To simulate the effect of past experience on the neural population, we modeled the "oblique effect," which describes the psychophysical finding that humans are more visually sensitive to contours that are vertically or horizontally orientated than obliquely oriented (12, 13). The oblique effect is thought to arise because cardinal (horizontal and vertical) orientations are more frequent in natural scenes than oblique orientations (14). Its neural basis may originate in primary visual cortex, reflecting a greater number of neurons preferring cardinal orientations or stronger evoked responses to cardinal than oblique orientations (15, 16). The oblique effect was modeled here by making c a sinusoidal function of orientation preference, $c(\theta) = c_0 - w_\theta \cdot \cos(4 \cdot \theta \cdot \pi/180)$, decreasing the baseline level of inhibition (c_0) for neurons with cardinal orientation preferences and increasing it for neurons with oblique orientation preferences (Fig. S4A). Here, c_0 is the baseline level of the suppressive field gain term, and w_θ is a weight that reflects the extent to which the suppressive field gain term has been modified by experience. Within the cosine function, θ is multiplied by 4 so that troughs in $c(\theta)$ occur at the cardinal orientations ($0°$ and $90°$), and peaks occur at the oblique orientations ($45°$ and $135°$). Incorporating the effect of prior experience, the response of each model complex cell to stimulus I is described by the equation

$$R(X,\theta) = \frac{D(X,\theta)}{\nu + c(\theta) \cdot S(X,\theta)}. \quad [7]$$

When the population activity is transformed into stimulus probabilities (see next section), $c(\theta)$ can be thought of as the neural representation of a Bayesian prior. The strength of the prior is reflected in the amplitude of $c(\theta)$. When $c(\theta)$ is constant ($w_\theta = 0$), the prior is flat (experience reveals all orientations are equally likely), and the neural responses are determined entirely by the sensory information represented in $D(X,\theta)$. When $c(\theta)$ varies sinusoidally (experience reveals that cardinal orientations are more likely than oblique orientations), the neural responses reflect both the sensory information and the prior. As the strength of the prior increases (the probability of encountering cardinal orientations increases), the amplitude of $c(\theta)$ is assumed to increase (i.e., w_θ increases) due to plasticity in the strength of lateral connectivity, resulting in a larger effect of the prior on the neural responses. To examine how the strength of the prior affects behavioral performance, we performed a simulation with $c_0 = 1\text{x}10^{-4}$ (the control value of c) and three values of w_θ: 0 (reflecting a flat prior), $2.5\text{x}10^{-5}$ (reflecting a weak prior), and $5\text{x}10^{-5}$ (reflecting a strong prior). Such changes in c are assumed to occur slowly over long time scales, reflecting the extensive experience necessary to establish statistical regularities about the world. As such, changes in c are not likely to underlie priors formed over short time periods. The effect of $c(\theta)$, and thus the prior, is to facilitate neural responses to cardinal orientations and attenuate responses to oblique orientations (Fig. S4B), modifying the tuning curves (17). Decoding the population activity reveals that the prior results in higher probabilities (greater certainty) about cardinal than oblique orientations (Fig. S4C). When the decoded population activity is used to discriminate changes in stimulus orientation, as described next, the greater certainty about cardinal orientations results in lower thresholds (better discriminability) at cardinal than oblique orientations (Fig. S5). The effect of the prior could also be observed in the baseline population activity of the model (i.e., during presentation of a stimulus defined by all zeros; Fig. S4D), consistent with data suggesting that visual experience increases the similarity of natural scene responses and baseline neuronal activity (18).

The behavioral measurement of orientation discrimination thresholds in a two interval forced-choice experiment was simulated using the neural network model with $c_0 = 1\text{x}10^{-4}$ and $w_\theta = 7.5\text{x}10^{-5}$. In one interval, a reference stimulus (e.g., $90°$) was presented, and in the other a test stimulus (e.g., $91°$) was presented. For both intervals, a probabilistic population code (see next section) was used to determine the most likely stimulus orientation. Reference orientations of $45°$ and $90°$ were used, with test orientations spanning $20°$ centered on each reference in $1°$ steps. Each combination of reference and test was presented 200 times. The proportion of times the test orientation was determined to be rotated counter-clockwise from the reference orientation was then computed, and a cumulative Gaussian fit to the data to calculate the threshold (the standard deviation of the Gaussian; Fig. S5).

Probabilistic Population Codes. A fundamental question in neural computation is how the activity of a population of neurons can be decoded to determine which stimuli are present in the environment, in turn allowing appropriate behavioral responses to be selected. One possibility is to interpret neuronal population activity as a probability distribution describing the likelihood of different possible stimuli, and to then act according to the most probable stimulus. The expression of neural activity as a probability distribution can be implemented using probabilistic population codes (PPCs), which relate population activity to a posterior probability distribution describing the probability with which each possible stimulus was presented (19-21). A PPC captures the intuition that higher activity in a subpopulation of neurons with similar stimulus preferences indicates greater certainty about the stimulus. As such, certainty about the presented stimulus increases with the gain of the population activity (the peak response amplitude) (Fig. S1). A key implication of a PPC is that task performance will be better when the gain of the population activity supporting that behavior is larger.

For the simulations in Figs. S1B, S4C, and S5, a PPC was used in decoding the population activity of the model neurons whose receptive fields were aligned with the visual stimulus. Specifically, given a population response $\boldsymbol{r}$ elicited by a stimulus with orientation θ, the posterior probability distribution, $p(\theta|\boldsymbol{r})$, was computed using the equation

$$p(\theta|\boldsymbol{r}) \propto \prod_i \frac{e^{-f_i(\theta)} \cdot f_i(\theta)^{r_i}}{r_i!} \cdot p(\theta). \quad [8]$$

Here, $f_i(\theta)$ is the tuning curve of the i^{th} neuron in the population, r_i is a single trial response assuming Poisson variability, and $p(\theta)$ (the probability of observing stimulus θ) is assumed to be flat. As discussed above, priors reflecting extensive experience (e.g., the oblique effect) are assumed to modify the tuning curves themselves (17). In contrast, more "short-term" priors (such as one created artificially in a psychophysical study by manipulating stimulus probabilities) are assumed to be reflected in $p(\theta)$. Because of the variability that occurs in $p(\theta|\boldsymbol{r})$ across trials, we performed the simulations $10{,}000$ times and took averages to produce the smooth curves in Fig. S1B and Fig. S4C. When a PPC is used in decoding neuronal population activity, the certainty about the presented stimulus increases with the population gain. As an example, population responses elicited by vertically oriented sinusoidal gratings of 7.5% and 20% contrast are shown in Fig. S1A. The corresponding posterior probability distributions computed from these responses are shown in Fig. S1B. Note that the larger amplitude response to a grating of 20% contrast results in a taller and narrower posterior probability distribution, indicating greater certainty about this stimulus compared to the 7.5% contrast stimulus (19).

Visual Stimuli. The visual stimuli used in the simulations were sinusoidal gratings and Gabor functions that varied in contrast, position, orientation, and size:

$$I(X,\theta) = a \cdot e^{-\frac{X_\theta^2}{2\sigma_I^2} - \frac{Y_\theta^2}{2\sigma_I^2}} \cdot \cos(\mathrm{SF} \cdot X_\theta). \quad [9]$$

Here, $X = (x, y)$ with x and y denoting the horizontal and vertical dimensions of retinotopic space, $X_\theta = \cos(\theta) \cdot (x - x_0) + \sin(\theta) \cdot (y - y_0)$ and $Y_\theta = -\sin(\theta) \cdot (x - x_0) + \cos(\theta) \cdot (y - y_0)$ where x_0 and y_0 determine the horizontal and vertical positions of the stimulus, a sets the contrast ($0 \leq a \leq 1$), σ_I sets the size, θ sets the orientation, and SF is the spatial frequency.

In Fig. 3B, a ranged from 0 to 1 in steps of 0.01, $\theta = 90°$, $x_0 = y_0 = 0°$, SF $= 5.75$ cyc/°, and $\sigma_I = 1.55°$. For the simulations in Fig. 3C, the stimuli were defined by summing two orthogonal Gabor functions. The first was at the neuron's preferred orientation ($\theta = 90°$) with $a = 0.5$, $x_0 = y_0 = 0°$, SF $= 5.75$ cyc/°, and $\sigma_I = 1.55°$. For the second Gabor function, a ranged from 0 to 0.5 in steps of 0.005, $\theta = 0°$, $x_0 = y_0 = 0°$, SF $= 5.75$ cyc/°, and $\sigma_I = 1.55°$. In Fig. 3D, $a = 1$, $\theta = 90°$, $x_0 = y_0 = 0°$, SF $= 5.75$ cyc/°, and σ_I ranged from $0.05°$ to $10.0°$ in steps of $0.1°$. In Fig. 4C, $a = 1$, $\theta = 90°$, $x_0 = y_0 = 0°$, SF $= 5.75$ cyc/°, and σ_I ranged from $1.55°$ to $6.05°$ in steps of $0.1°$. In Fig. 4D, a ranged from 0 to 1 in steps of 0.01, $\theta = 90°$, $x_0 = y_0 = 0°$, SF $= 5.75$ cyc/°, and $\sigma_I = 1.55°$. In Fig. 5 C and D, $a = 1$, $\theta = 90°$, x_0 ranged from $0°$ to $10°$ in steps of $0.2°$,

$y_0 = 0°$, SF = 5.75 cyc/°, and $\sigma_I = 1.55°$. In Fig. S1, either $a = 0.075$ (7.5%) or $a = 0.2$ (20%), θ ranged from $0°$ to $180°$ in $0.25°$ steps, $x_0 = y_0 = 0°$, SF = 3 cyc/°, and $\sigma_I = 1.55°$. In Fig. S2, the stimulus parameters were the same as in Fig. 4. In Fig. S3, the stimulus parameters were the same as in Fig. 5, with the exception that $a = 0.1$ in Fig. S3 B and C. In Fig. S4B, $a = 0.1$, $\theta = 45°$ (dashed lines) or $\theta = 90°$ (solid lines), $x_0 = y_0 = 0°$, SF = 3 cyc/°, and the stimuli were not Gaussian-enveloped. In Fig. S4C, $a = 0.1$, θ ranged from $0°$ to $180°$ in $1°$ steps, $x_0 = y_0 = 0°$, SF = 3 cyc/°, and the stimuli were not Gaussian-enveloped. In Fig. S5, $a = 0.05$, $x_0 = y_0 = 0°$, SF = 3 cyc/°, and the stimuli were not Gaussian-enveloped.

Psychophysical Data. Psychophysical data on the perceptual consequences of autism were extracted from previously published papers (22, 23) using a graph-tracing program (24).

SI FIGURES

Figure S1

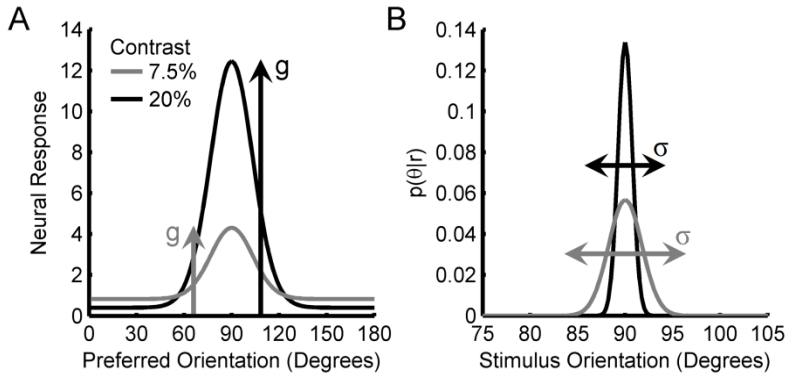


Fig. S1. Probabilistic population codes. (*A*) Population activity of the V1 typically developing control model elicited by vertically oriented sinusoidal gratings with contrasts of 7.5% (gray) and 20% (black). Along the x-axis, neurons are rank ordered according to their preferred orientation. The response of each neuron is plotted on the y-axis. The peaks at 90° reflect that the stimuli were vertically oriented. Note that the higher contrast stimulus elicits a higher amplitude population response than the lower contrast stimulus. The amplitude (height) of the population activity, indicated by the vertical arrow, is referred to as the population gain (g). (*B*) A probabilistic population code was used to compute posterior probability distributions, $p(\theta|\boldsymbol{r})$, over stimulus orientation (θ) given the population responses ($\boldsymbol{r}$) shown in *A*. Note that the population gain is inversely related to the width (σ) of the posterior probability distribution, and therefore directly related to the certainty about the presented stimulus. For example, the larger amplitude population response to a stimulus with 20% contrast translates into a taller and narrower $p(\theta|\boldsymbol{r})$ indicating higher certainty, whereas the smaller amplitude population response to a stimulus with 7.5% contrast translates into a shorter and wider $p(\theta|\boldsymbol{r})$ indicating lower certainty.

Figure S2

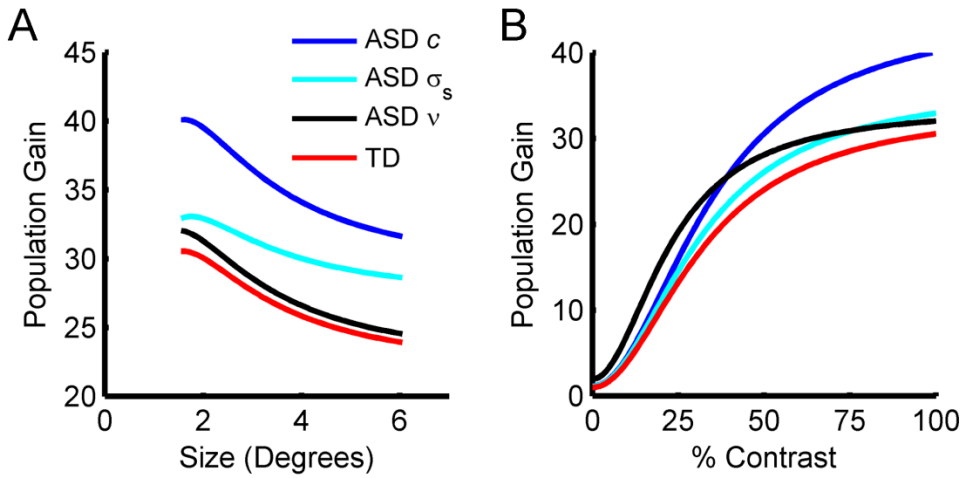


Fig. S2. Simulation 1: visual spatial suppression (Fig. 4). Comparing the effects of changing c, ν, and σ_S on visual spatial suppression. (*A*) Population gain as a function of stimulus size for high contrast stimuli. For the typically developing control model (TD; red curve reproduced from Fig. 4C), the divisive normalization parameters are: $c = 1\text{x}10^{-4}$, $\nu = 1$, and $\sigma_S = \sqrt{5}°$. For the autism model with altered suppressive field gain term (ASD c; blue curve from Fig. 4C), the parameters are: $c = 7.5\text{x}10^{-5}$ (75% of the control value), $\nu = 1$, and $\sigma_S = \sqrt{5}°$. For the autism model with altered semisaturation constant (ASD ν; black), the parameters are: $c = 1\text{x}10^{-4}$, $\nu = 0.01$ (1% of the control value), and $\sigma_S = \sqrt{5}°$. Despite the large change in ν, the effect on the population gain is minimal. For the autism model with reduced neuronal pooling (ASD σ_S; cyan), the parameters are: $c = 1\text{x}10^{-4}$, $\nu = 1$, and $\sigma_S = 0.8 \cdot \sqrt{5}°$ (80% of the control value). Decreasing the extent of neuronal pooling results in larger population gains due to an increased E/I ratio, and attenuates the rate at which spatial suppression occurs as the stimulus size increases (the curve is flatter) since neurons with more distal receptive fields contribute less to the divisive normalization pool. (*B*) Population gain as a function of stimulus contrast for small stimuli. The TD and ASD c curves are reproduced from Fig. 4D. The change in σ_S for the ASD σ_S model has a similar qualitative effect as the change in c, but the magnitude of the effect is smaller. The change in ν for the ASD ν model results in a leftward pull in the population gain (c.f., Fig. 2A) that would improve contrast sensitivity. The finding that contrast sensitivity is unaffected in autism (25) thus suggests that in the dark adapted state in which contrast sensitivity is measured, ν is unaffected. However, it is interesting to speculate that sensory hypersensitivity in autism (26) may be related to deficits in gain control (dynamic changes in ν). It is thus possible that steady-state values of ν are not altered in autism, but the dynamic process in which ν changes according to recent sensory stimulation is impaired.

Figure S3

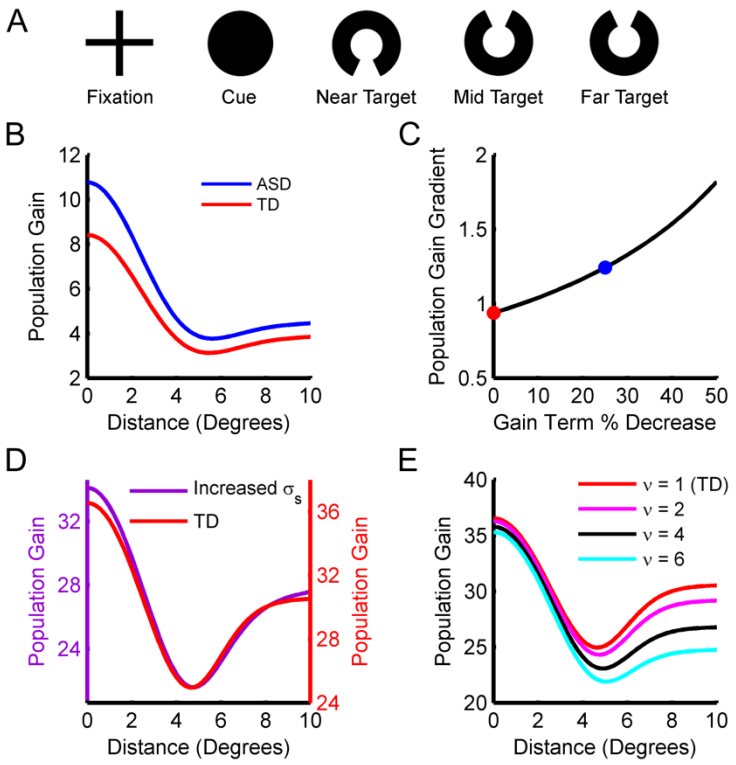


Fig. S3. Simulation 2: tunnel vision (Fig. 5). (*A*) Mapping the gradient of attention. On each trial, fixation was maintained while a cue was first flashed to capture attention at that location, and a target then briefly presented at a near, mid, or far distance from the cue. Subjects reported if there was an opening at the bottom (illustrated for the near location) or top (illustrated for mid and far locations) of the target (23). (*B*,*C*) Results for the typically developing control (TD) and autism (ASD) models presented in the main text, but with a stimulus contrast of 0.1 rather than 1.0. (*B*) Population gain as a function of target distance from the cue. The reduced stimulus contrast roughly equates the population gains of the two models at the largest distances (where the attentional field has little to no effect). The gradient of the population gain is steeper for the autism than the control model. (*C*) Results showing that as the suppressive field gain term decreases (simulating an increasing degree of autism symptomatology), the gradient of the population gain increases as in Fig. 5D, which is consistent with the psychophysical findings of Robertson et al. (2013) (23). The colored dots correspond to the control and autism models in *B*. (*D*,*E*) Effects of changing σ_S and ν on the gradient of attention. (*D*) Population gain as a function of target distance from the cue. For the TD curve (red; reproduced from Fig. 5C), the divisive normalization parameters are: $c = 1\text{x}10^{-4}$, $\nu = 1$, and $\sigma_S = \sqrt{5}°$. To achieve a steeper gradient in the population gain through a manipulation of σ_S, it was necessary to decrease the E/I ratio by increasing the extent of neuronal pooling (purple curve; here, $\sigma_S = 1.5 \cdot \sqrt{5}°$). To highlight the gradient of the population gain, the *y*-axes are shifted to align the troughs of the two curves. The difference between minimum and maximum values on the two *y*-axes is the same. (*E*) Population gain as a function of target distance from the cue. The TD curve is reproduced from Fig. 5C. To achieve a steeper gradient in the population gain through a change in ν, it was necessary to decrease the E/I ratio by increasing the semisaturation constant. Note that increasing ν has a small effect on the maximum of the population gain, but deepens the trough, resulting in a steeper gradient of attention.

Figure S4

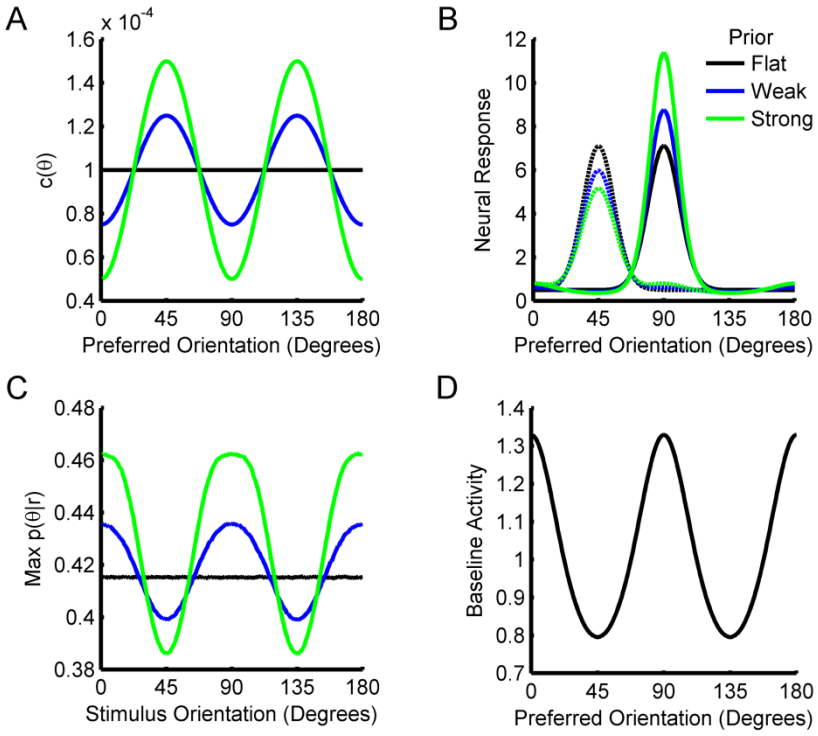


Fig. S4. Simulation 3: implementation of Bayesian priors. (*A*) The suppressive field gain term, $c(\theta)$, is shown for three conditions: (*i*) flat prior (black) in which all stimulus orientations are equally likely, (*ii*) a weak prior in which cardinal orientations are somewhat more likely than oblique orientations (blue), and (*iii*) a strong prior in which cardinal orientations are much more likely than oblique orientations (green). Troughs in $c(\theta)$ correspond to the most likely orientations and peaks correspond to the least likely. The strength of the prior is reflected in the amplitude of $c(\theta)$. The extent to which experience changes the shape of c may be attenuated in autism. For the oblique effect, this would result in a lower amplitude of $c(\theta)$ for individuals with autism (e.g., the blue curve) than typically developing peers (e.g., the green curve). As a consequence, there may be a reduced influence of Bayesian priors on behavior in autism (9), consistent with results suggesting that the oblique effect is diminished in the disorder (13). (*B*) Population activity elicited by vertically (solid lines) and obliquely (dotted lines) oriented gratings. Along the x-axis, neurons are rank ordered according to their preferred orientation. The response of each neuron is plotted on the y-axis. When the prior is flat, the gain of the population activity is the same for vertical and oblique stimuli. A non-flat prior facilitates responses to cardinal orientations and attenuates responses to oblique orientations. (*C*) Maximum of the posterior probability distribution, $p(\theta|\boldsymbol{r})$, for each stimulus orientation (θ) computed from the corresponding population response ($\boldsymbol{r}$). When the prior is flat, the maximum of $p(\theta|\boldsymbol{r})$ is independent of stimulus orientation. A non-flat prior increases the maximum of $p(\theta|\boldsymbol{r})$ for cardinal orientations and reduces it for oblique orientations. These changes in $p(\theta|\boldsymbol{r})$ lead to smaller psychometric thresholds for cardinal than oblique orientations (Fig. S5). (*D*) The effect of the prior can also be observed in the baseline population activity. The curve shows the baseline activity of all model complex cells with receptive fields located at $x_0 = 0°$ (with $w_\theta = 5\text{x}10^{-5}$), rank-ordered by their orientation preference. The baseline activity of neurons preferring cardinal orientations is slightly higher than that of neurons preferring oblique orientations.

Figure S5

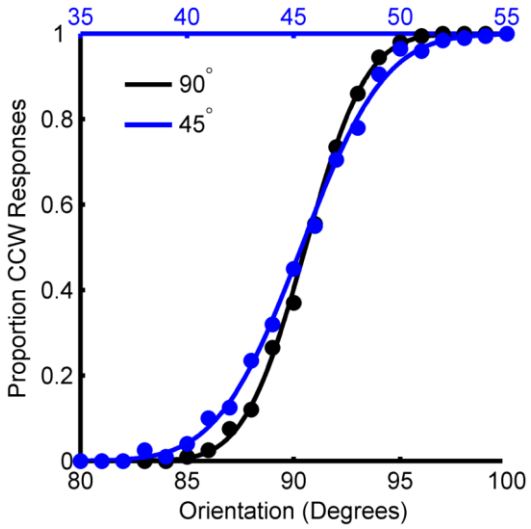


Fig. S5. Simulation 3: simulated psychometric functions illustrating the oblique effect. The ability of the model with a prior for cardinal orientations to discriminate small changes in stimulus orientation was tested at cardinal (90°; black) and oblique (45°; blue) reference orientations. The proportion of times that a test orientation was determined to be rotated counter-clockwise (CCW) relative to the reference is plotted as a function of the test orientation (indicated on the *x*-axes). The psychometric function measured at 90° is steeper than the one measured at 45°, indicating greater sensitivity to small changes in orientation at cardinal than oblique orientations.

SI REFERENCES

1. Adelson EH & Bergen JR (1985) Spatiotemporal energy models for the perception of motion. *J Opt Soc Am A* 2(2):284-299.
2. Zhang JX, Rosenberg A, Mallik AK, Husson TR, & Issa NP (2007) The representation of complex images in spatial frequency domains of primary visual cortex. *J Neurosci* 27(35):9310-9318.
3. Issa NP, Rosenberg A, & Husson TR (2008) Models and measurements of functional maps in V1. *J Neurophysiol* 99(6):2745-2754.
4. Heeger DJ (1992) Normalization of cell responses in cat striate cortex. *Vis Neurosci* 9(2):181-197.
5. Heeger DJ & Simoncelli EP (1993) Model of visual motion sensing. *Spatial vision in humans and robots* 19:367-392.
6. Simoncelli EP & Heeger DJ (1998) A model of neuronal responses in visual area MT. *Vision Res* 38(5):743-761.
7. Reynolds JH & Heeger DJ (2009) The normalization model of attention. *Neuron* 61(2):168-185.
8. Qian N & Lipkin RM (2011) A learning-style theory for understanding autistic behaviors. *Front Hum Neurosci* 5:77.
9. Pellicano E & Burr D (2012) When the world becomes 'too real': A Bayesian explanation of autistic perception. *Trends Cogn Sci* 16(10):504-510.
10. Sinha P, Kjelgaard MM, Gandhi TK, Tsourides K, Cardinaux AL, Pantazis D, Diamond SP, & Held RM (2014) Autism as a disorder of prediction. *Proc Natl Acad Sci U S A* 111(42):15220-15225.
11. Schwartz O & Coen-Cagli R (2013) Visual attention and flexible normalization pools. *J Vis* 13(1):25.
12. Westheimer G & Beard BL (1998) Orientation dependency for foveal line stimuli: Detection and intensity discrimination, resolution, orientation discrimination and Vernier acuity. *Vision Res* 38(8):1097-1103.
13. Dickinson A, Jones M, & Milne E (2014) Oblique orientation discrimination thresholds are superior in those with a high level of autistic traits. *J Autism Dev Disord* 44(11):2844-2850.
14. Coppola DM, Purves HR, McCoy AN, & Purves D (1998) The distribution of oriented contours in the real world. *Proc Natl Acad Sci U S A* 95(7):4002-4006.
15. Furmanski CS & Engel SA (2000) An oblique effect in human primary visual cortex. *Nat Neurosci* 3(6):535-536.
16. Li B, Peterson MR, & Freeman RD (2003) Oblique effect: A neural basis in the visual cortex. *J Neurophysiol* 90(1):204-217.
17. Ganguli D & Simoncelli EP (2014) Efficient sensory encoding and Bayesian inference with heterogeneous neural populations. *Neural Comput* 26(10):2103-2134.
18. Berkes P, Orban G, Lengyel M, & Fiser J (2011) Spontaneous cortical activity reveals hallmarks of an optimal internal model of the environment. *Science* 331(6013):83-87.
19. Ma WJ, Beck JM, Latham PE, & Pouget A (2006) Bayesian inference with probabilistic population codes. *Nat Neurosci* 9(11):1432-1438.
20. Beck JM, Latham PE, & Pouget A (2011) Marginalization in neural circuits with divisive normalization. *J Neurosci* 31(43):15310-15319.
21. Seilheimer RL, Rosenberg A, & Angelaki DE (2014) Models and processes of multisensory cue combination. *Curr Opin Neurobiol* 25:38-46.
22. Foss-Feig JH, Tadin D, Schauder KB, & Cascio CJ (2013) A substantial and unexpected enhancement of motion perception in autism. *J Neurosci* 33(19):8243-8249.
23. Robertson CE, Kravitz DJ, Freyberg J, Baron-Cohen S, & Baker CI (2013) Tunnel vision: Sharper gradient of spatial attention in autism. *J Neurosci* 33(16):6776-6781.
24. Tummers B (2006) DataThief III. Available at datathief.org/.
25. Koh HC, Milne E, & Dobkins K (2010) Spatial contrast sensitivity in adolescents with autism spectrum disorders. *J Autism Dev Disord* 40(8):978-987.
26. Tomchek SD & Dunn W (2007) Sensory processing in children with and without autism: A comparative study using the short sensory profile. *Am J Occup Ther* 61(2):190-200.